
This is an electronic reprint of the original article.
This reprint may differ from the original in pagination and typographic detail.

Schröder, Philipp; Schröder, Philipp; Aguiló-Aguayo, Noemí; Auer, Andrea; Grießer, Christoph; Kunze-Liebhäuser, Julia; Ma, Yibo; Hummel, Michael; Obendorf, Dagmar; Bechtold, Thomas

Activation of carbon tow electrodes for use in iron aqueous redox systems for electrochemical applications

Published in:
Journal of Materials Chemistry C

DOI:
[10.1039/d0tc00594k](https://doi.org/10.1039/d0tc00594k)

Published: 21/06/2020

Document Version
Peer-reviewed accepted author manuscript, also known as Final accepted manuscript or Post-print

Please cite the original version:
Schröder, P., Schröder, P., Aguiló-Aguayo, N., Auer, A., Grießer, C., Kunze-Liebhäuser, J., Ma, Y., Hummel, M., Obendorf, D., & Bechtold, T. (2020). Activation of carbon tow electrodes for use in iron aqueous redox systems for electrochemical applications. *Journal of Materials Chemistry C*, 8(23), 7755-7764.
<https://doi.org/10.1039/d0tc00594k>

This material is protected by copyright and other intellectual property rights, and duplication or sale of all or part of any of the repository collections is not permitted, except that material may be duplicated by you for your research use or educational purposes in electronic or print form. You must obtain permission for any other use. Electronic or print copies may not be offered, whether for sale or otherwise to anyone who is not an authorised user.

Activation of carbon tow electrodes for use in iron aqueous redox systems for electrochemical applications

Philipp Schröder^{a,b,e}, Noemí Aguiló-Aguayo^b, Andrea Auer^c, Christoph Griesser^c, Julia Kunze-Liebhäuser^c, Yibo Ma^d, Michael Hummel^d, Dagmar Obendorf^a, Thomas Bechtold^{b*}

Received 00th January 20xx,
Accepted 00th January 20xx

DOI: 10.1039/x0xx00000x

Excellent chemical inertness, good conductivity and high overpotentials for water electrolysis make carbon fibres (CFs) an ideal electrode material for electrochemical applications. A customized design of three-dimensional (3D) carbon electrodes can be achieved by tailored fibre placement of carbon tows with textile production techniques like embroidery. After manufacturing of the 3D structure, appropriate removal of the polymer coating and oxidative activation is required to achieve low overpotentials and avoiding thermal treatments of the carbon structure. For the electrolytes Na[Fe^{III}-racEDDHA] and K₄[Fe^{II}(CN)₆] a sequential treatment by acetone extraction and anodic oxidation was identified to yield optimum surface activation. Electron microscopy, Raman spectroscopy and X-ray photoelectron spectroscopy of activated fibres indicated complete removal of the coating layer without damage of the CFs. From electrochemical impedance spectroscopy (EIS) at the carbon tow electrodes, charge transfer resistances of < 0.1 Ω (0.023 Ω g) and < 0.2 Ω (0.046 Ω g) were determined at 50% state-of-charge (SoC) for 65 mM K₄[Fe^{II}(CN)₆] and 65 mM Na[Fe^{III}-racEDDHA], respectively. In potentiostatic bulk electrolysis no electrode deactivation was observed during 10 charge/discharge cycles (5-6 hours) between 10% and 90% SoC. The processing of carbon tows by textile techniques to near net shaped 3D electrodes opens a new method to manufacture electrodes for electrochemical applications, such as redox flow cells.

1. Introduction

Carbon-based electrodes, such as carbon fibres (CFs), feature high flexibility, good conductivity, large overpotential towards hydrogen and oxygen evolution, and corrosion resistance. Thus, CF based electrodes have been investigated extensively as electrode material for use in energy storage and environmental applications.^{1,2} For instance, porous electrodes based on carbon felt and CF based fabric were used in redox flow cells.^{3,4} Successful use of activated carbon cloth also has been reported for capacitive deionisation in water desalination,^{5,6} also employed without an additional current collector.⁵

In electrochemical applications, polarisation losses due to activation and concentration overpotentials are responsible for the poor performance of electrochemical reactors. The electrode surface functionality and porous structure may enhance the charge transfer at the interface electrode/electrolyte and the mass transport of the reactants and products within the electrodes.

Carbon surfaces often exhibit poor electrochemical characteristics⁷ and therefore need special pretreatment, frequently termed as “activation”. For surface sensitive redox couples⁸ the electron transfer at carbon electrodes may depend on edge plane exposure,⁹ surface functional groups¹⁰ and cleanliness.¹¹ Porous electrode structures, such as carbon felts and carbon papers composed of randomly oriented CFs, also suffer from poor electrolyte accessibility, high pressure drops within the cell, and non-uniform electrolyte velocities.^{12,13} These issues limit the mass transport, for instance in redox flow cells, and thus their electrochemical performance. Some improvements have been achieved by modifying the cell architecture (by adding flow fields) and the electrode design.^{14,15} Another strategy is to employ electrodes that allow for control of the orientation of their fibres along the electrolyte flow.¹⁶

Recently, embroidery techniques have emerged as useful method to manufacture conductive structures for application in batteries and RFCs.^{17,18} 3D structures can be formed as near net-shaped elements and cutting to the final shape is no longer necessary. By use of the so-called soutache technique threads from conductive material e.g. metal wire or carbon tows, often termed carbon fibre rovings, can be placed on a textile support according to the planned design of an electrode (Fig. 1). Through this tailored fibre

^a Institute of Analytical Chemistry and Radiochemistry, Leopold-Franzens-University Innsbruck, Innrain 80-82, 6020 Innsbruck, Austria.

^b Research Institute of Textile Chemistry and Textile Physics, Leopold-Franzens-University of Innsbruck, Hoehsterstraße 73, 6850 Dornbirn, Austria.

*Corresponding author. E-mail: Thomas.bechtold@uibk.ac.at, textilchemie@uibk.ac.at

^c Department of Physical Chemistry, Leopold-Franzens-University Innsbruck, Josef-Möller-Haus, Innrain 52c, 6020 Innsbruck, Austria.

^d Department of Bioproducts and Biosystems, Aalto University, Vuorimiehentie 1, 02150 Espoo, Finland.

^e Austrian Drug Screening Institute – ADSI, University of Innsbruck, Innrain 66a, 6020 Innsbruck, Austria.

† Footnotes relating to the title and/or authors should appear here.

Electronic Supplementary Information (ESI) available: [from ESI-1 to ESI-10]. See DOI: 10.1039/x0xx00000x

placement, the density and direction of CF rovings on the support can be adjusted according to current density and hydraulic requirements.

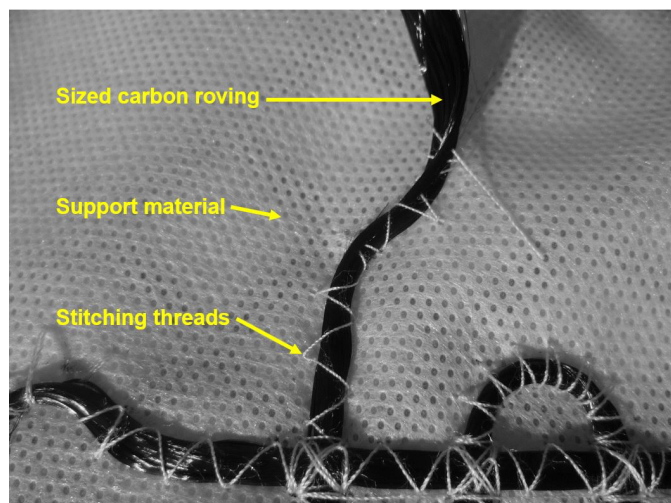


Fig. 1. Embroidered carbon electrode structure.

While the direct use of technically available CF rovings opens access to new electrode designs, commercial CF rovings are typically designed to be used in composite materials and cannot readily be adopted for electrochemical purposes without pretreatment. In the manufacturing process, commercial CF rovings are processed to improve the bonding properties between fibre and composite matrix.¹⁹ Surface modification usually implies oxidative treatment, such as chemical, electrochemical or plasma treatment.²⁰ Additionally, the CF rovings are coated by a polymer layer (typically termed sizing) in order to protect and align the fibres, increase the inter-filamentary adhesion, lubricate the fibres for textile processing, and to dissipate electrostatic charge.²¹ Typical sizing formulations include polymers like epoxy, polyester, urethane and other components as lubricant, wetting and antistatic agents. For electrochemical purposes the roving has to be desized²² after the textile processing step. The intrinsic advantages of CF rovings could be utilized if appropriate methods for removal of the sizing and surface activation are available after the full electrode structure had been formed e.g. by embroidery techniques.

The following criteria has to be targeted for the activation process:

- High electrochemical activity.
- Time stable electrochemical response.
- Applicable to embroidered 3D electrodes, which contain non-conductive, heat-sensitive fibres as supporting material, e.g. polypropylene, polyamide fibres.
- No damage of fibre matrix, thus retention of conductivity.
- “Green” method avoiding toxic chemicals.

Among different procedures, which are typically used to activate carbon-based electrodes (e.g. thermal treatment,^{23,24} chemical oxidation,^{25,26} decoration with MWCNTs^{27,28}), electrochemical activation methods are required to be applied to embroidered electrodes meeting the demands classified above. A wide range of different procedures has been investigated to treat carbon-based

materials with electrochemical methods.^{29–31} Anodic treatment in acidic media leads to an amorphous layer of graphite oxide.³² Dissolution of graphite oxide flakes and a relatively low surface oxygen content was observed after anodic polarisation in an alkaline electrolyte.³³

In this work we present a study of desizing and activation methods applied to CF rovings for use in electrochemical applications, such as redox flow cells. The recently described non-toxic, aqueous, all-iron redox flow system^{34,35} ferro/ferricyanide [$\text{Fe}^{\text{II/III}}(\text{CN})_6$] and iron(II/III)-N,N'-ethylene-bis-(o-hydroxyphenylglycine) [$\text{Fe}^{\text{II/III}}\text{-racEDDHA}$], and a standard modulus polyacrylonitrile-based CF were used as model system. Voltammetric experiments showed good reversibility for both redox carriers at electrodes made from single CFs and glassy carbon (GC). A carbon roving loop electrode (CRLE) served as a simple model for embroidered 3D electrodes. The electrochemical performance of differently pretreated CRLEs was evaluated with electrochemical impedance spectroscopy (EIS) and their electrochemical stability was tested in charge/discharge cycling experiments for both redox couples separately. X-ray photoelectron spectroscopy (XPS), Raman spectroscopy, thermogravimetric analysis (TGA), and scanning electron microscopy (SEM) permitted to monitor changes of the roving surface during desizing and activation.

2. Experimental section

2.1. Chemicals

Na_2SO_4 , H_3BO_3 , NaOH , $\text{K}_3[\text{Fe}^{\text{III}}(\text{CN})_6]$, $\text{K}_4[\text{Fe}^{\text{II}}(\text{CN})_6]$, H_2SO_4 96% wt. and $\text{K}_2\text{Cr}_2\text{O}_7$, were purchased from Sigma-Aldrich in p.a. quality. $\text{Na}[\text{Fe}^{\text{III}}\text{-racEDDHA}]$ was isolated from commercial fertilizer (Basafer Plus, Compo Expert, 6% wt $\text{Na}[\text{Fe}^{\text{III}}\text{-EDDHA}]$). Epoxy resin 105 and fast hardener 205 were purchased from West System (Geugeon Brothers, Inc., Michigan). CFs were purchased from Toho Tenax (STS 40, 48 k, 3200 tex, 1% PU sizing, Toho Tenax Europe, Heinsberg, Germany). The isolation of the $\text{Na}[\text{Fe}^{\text{III}}\text{-racEDDHA}]$ complex was performed according to the procedure published in the literature.³⁵ In brief, approx. 500 ml hot ethanol extract of crude fertilizer was evaporated to dryness. The residue was dissolved in 100 ml 70% vol EtOH and applied to a 30 x 6 cm basic aluminium oxide column. The brick red $\text{Na}[\text{Fe}^{\text{III}}\text{-racEDDHA}]$ fraction was collected after 1500 sec elution with 70% vol EtOH and evaporated to dryness. 4.3 g $\text{Na}[\text{Fe}^{\text{III}}\text{-racEDDHA}]$ were obtained as a red solid. The purity of 95.6% wt. was determined via photometry from the absorbance of an aqueous solution and the molar absorptivity³⁵ at 480 nm ($\epsilon = 5026 \text{ L mol}^{-1} \text{ cm}^{-1}$) using Beer's law.

2.2. Electrode manufacturing and desizing

Desizing. Standard modulus CFs (STS40 48k, Toho Tenax, Japan) were extracted with acetone for 48 hours in a Soxhlet extractor. For preparation of the carbon fibre microcylinder electrodes (CFMCEs) a bundle of approx. 500 - 1000 desized fibres was inserted into a glass capillary (inner diameter 0.6 mm, outer diameter 5 mm). One fibre was pulled out of the fibre bundle (5 - 10 mm) with a micro forceps. In this way a single fibre protruding from the capillary, leaving the bulk of the fibres inside was produced. The capillary was then sealed

with a single drop of epoxy resin. Electrical connection was established at the far end of the capillary (Fig. 2a).

For preparation of the carbon roving loop electrodes (CRLEs) a carbon roving was inserted into 12 cm glass tubing (inner diameter 3 mm, outer diameter 5 mm), the end of the roving was guided back into the tubing forming a loop of an overall length of 72 mm (Fig. 2b).



Fig. 2. CF electrodes used in this work: a) carbon fibre microcylinder electrode (CFMCE), b) carbon roving loop electrode (CRLE).

After desizing for 48 hours in a Soxhlet extractor, the fibres got dispersed and behaved fluffy and unruly (ESI-1). The acetone was removed from the Soxhlet extract, the remaining residue represented 1% of the initial fibre mass. A Fourier-transform infrared (FT-IR) spectrum of the residue is depicted in (ESI-2). Additional TGA experiments with untreated, desized and activated fibres showed a loss of 1% wt. between 260°C and 380°C for the untreated sample which was absent for the treated samples (ESI-3).

In order to immobilize the carbon loop a small amount of epoxy resin was injected into the end of capillary. Special care was taken to avoid flow of resin into the carbon loop by “crimping” the cable with cable tie at the capillary outlet. Electrical contact was established at the far end of the tubing. For each electrode, the ohmic resistance of the electrode was calculated from the length of the roving l , resistivity of the roving $\rho = 0.000016$ ohm·m (provided by the supplier), and the cross sectional area A of the roving, which was calculated from the number of fibres per roving $n = 48000$ and the fibre radius $r = 3.5$ μm (Eq. 1).

$$R = \frac{\rho l}{r^2 \pi n} \quad (1)$$

Electrode activation. Chromic acid activation of CFMCE and CRLE was performed by immersion of the electrodes in chromic acid (10 g K_2CrO_4 /100 ml H_2SO_4 96% wt.) at ambient temperature. After 45 min reproducible results were obtained. Longer treatment did not further improve the electrochemical response.

For electrochemical activation of the CRLE two electrodes were placed in a beaker in a distance of approximately 10 cm. A reference electrode (Ag/AgCl 3 M KCl) was placed in close proximity to the electrode to be activated. The second CRLE served as inert counter electrode. In screening experiments different activation potentials and polarisation time were tested at room temperature using 0.1 M NaOH as electrolyte (the results are shown in ESI-7). Polarisation at 1800 mV for 90 s yielded the best electrode performance at short activation time.

Table 1. Experimental conditions applied for CRLE activation.

Method	Composition	Temperature	Time
Acetone extraction	Acetone	50 – 55 °C	48 h
Chemical oxidation	10 g K_2CrO_4 100 ml H_2SO_4 96% wt.	RT	45 min
Anodic oxidation	1800 mV 0.1 M NaOH	RT	90 s

2.4. Electrochemical characterization

Square wave voltammetry (SWV) and cyclic voltammetry (CV). A Metrohm VA663 stand connected to a software controlled potentiostat (PGSTAT302, Nova 1.11.2, Autolab, Netherlands) was used to perform the measurements.

Cyclic voltammograms (CVs) were recorded at a scan rate of 100 mVs^{-1} with a resolution of 1 mV. A planar 5 mm glassy carbon electrode (GCE) (Metrohm, Herisau, Switzerland) was used as working electrode and polished on a micro cloth (Buehler, Lake Bluff, USA) with 0.05 μm alumina (Buehler) prior each set of experiments. A Pt rod served as counter electrode and Ag/AgCl 1 M NaCl as reference electrode.

SWV was conducted at CFMCE as working electrode, Pt rod as counter electrode and Ag/AgCl 1M NaCl as reference electrode, with an amplitude of 50 mV, a frequency of 10 Hz and a step potential of 1 mV.

All voltammograms were started in the cathodic direction for 1 mM $\text{Na}[\text{Fe}^{\text{III}}\text{-racEDDHA}]$ electrolyte and in the anodic direction in the case of 1 mM $\text{K}_4[\text{Fe}^{\text{II}}(\text{CN})_6]$ electrolyte. A solution of 1 M Na_2SO_4 and 5 mM borate at pH 9 was used as background electrolyte.

Charge-discharge cycling experiments. A homemade 150 ml six neck round bottom flask was equipped with a CRLE, a reference electrode (Ag/AgCl 1M NaCl), a redox electrode (Pt // Ag/AgCl 3 M KCl), a modified phototrode (Metrohm 662 photometer), a glass U-tube filled with electrolyte and sealed at both ends with sintered glass frits of porosity P2, and an Ar inlet (ESI-4). Electrolysis was conducted with the PGSTAT302 potentiostat. The redox potential (E_{sol}) was simultaneously measured with a PGSTAT101 potentiostat. The tip of the phototrode was modified to permit reduction of the path length in the electrolyte down to approx. 50 μm . By this modification, direct quantification of the intensively coloured $[\text{Fe}^{\text{III}}\text{-racEDDHA}]$ and $[\text{Fe}^{\text{II}}(\text{CN})_6]$ in the electrolyte up to concentrations of 100 mM could be achieved (Fig. 3).

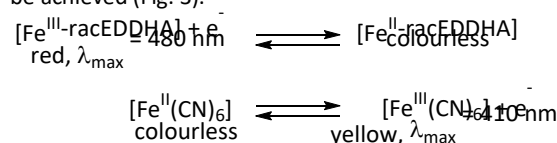


Fig. 3. Reaction scheme and absorbance characteristics of both redox carriers.

The modified phototrode was calibrated with $\text{Na}[\text{Fe}^{\text{III}}\text{-racEDDHA}]$ dissolved in 1 M Na_2SO_4 , pH 9, 50 mM borate or $\text{K}_3[\text{Fe}^{\text{II}}(\text{CN})_6]$ in 1 mM borate pH 9 using a reference device (Jenway Genova

spectrophotometer). The solution was agitated by a magnetic stirrer (Metrohm 728, Herisau, Switzerland) with 500–1800 rpm to achieve diffusion controlled electrode reactions. A 100 ml flask filled with the supporting electrolyte was used as the second half-cell, equipped with a 2x4 cm² Pt net counter electrode and agitated by a magnetic stirrer. Both half-cells were connected with the U-tube filled with supporting electrolyte (1 M Na₂SO₄).

The electrolyte concentration was set to 10 mM electroactive complex and charge-discharge cycling experiments were controlled galvanostatically (50 mA). Charge and discharge limits (10% and 90% State-of-Charge, SoC) were triggered by the Metrohm 662 photometer connected the analog input of the PGSTAT302 potentiostat. In case of [Fe^{II/III}-racEDDHA] additional potential limits (charge -1250 mV / discharge 100 mV) were set in order to prevent undesired side reactions. The electrode overpotential η was calculated from the potential difference between the working electrode (E_{we}) and a redox electrode (E_{sol}) (Pt // Ag/AgCl 3 M KCl) at 50% SoC (Eq. 2) placed in the solution. The averaged overpotential $\bar{\eta}$ was calculated from charge/discharge overpotentials and corrected for the potential drop caused by the roving resistance R_{rov} at charge/discharge current (Eq. 3).

$$\eta = E_{we} - E_{sol} \quad (2)$$

$$\bar{\eta} = \frac{|\eta_{charge}| + |\eta_{discharge}|}{2} - R_{rov} \times |I| \quad (3)$$

Influence of electrolyte convection on the overpotential was minimised through adjustment of a sufficiently high stirring speed (ESI-5). The reference electrode was positioned in short distance to the working electrode, thus contribution of the potential drop from the electrolyte solution resistance was minimised.

EIS experiments. The electrolyte 65 mM Na[Fe^{III}-racEDDHA], 0.7 M Na₂SO₄, 155 mM borate pH 9, was reduced at the negative electrode to reach 50% SoC (determined by photometry), using the same setup outlined in the charge-discharge cycling experiments. Potassium ferro/ferricyanide at 50% SoC was directly prepared with 32.5 mM K₃[Fe^{III}(CN)₆], 32.5 mM K₄[Fe^{II}(CN)₆], 0.7 M Na₂SO₄, 1 mM borate, pH 9. Three-electrode configuration with two CRLEs used as working and counter electrode and a reference electrode (Ag/AgCl 3 M KCl) were connected to a BioLogic VSP potentiostat. The impedance spectra were recorded from 3·10⁴ Hz to 5·10⁻² Hz. An AC amplitude of 100 mV was applied on top of a DC potential matching the open cell potential at 50% SoC. All electrodes used had a similar roving length (72 mm) and weight (0.23 g).

2.5. Surface characterisation

XPS. A Multilab 2000 (Thermo Scientific) instrument was used, comprising a hemispherical sector analyser (Alpha 110, Thermo Scientific) and a monochromatised Al K α X-ray source (1486.6 eV). For charge compensation, electrons with a kinetic energy of 6 eV were provided via a flood gun. Prior to every measurement, the samples were pressed into an indium matrix. For the calibration of the binding energy, the In 3d_{5/2} peak was used (440 eV). The high resolution spectra of the C 1s, O 1s, N 1s regions were collected at a pass energy of 25 eV and an energy step size of 0.05 eV.

For peak fitting, a Shirley-type background was applied for all regions. Peak deconvolution of the C 1s region was performed by employing a mixed Gaussian-Lorentzian peak shape (GL 30) for all components except for the sp² carbon, where an asymmetric function³⁶ was applied (asymmetry index: 0.11). For the semi-quantitative analysis of the C 1s, O 1s and N 1s regions, they were corrected by their relative sensitivity factors and by the escape depths of the electrons utilizing the Gries equation.³⁷

Raman. The spectra were collected using a LabRAM HR (HORIBA) equipped with a charge couple detector. A 514 nm Ar laser was exposed 60 s on a sample at 0.1% laser power. Two scans were collected using a 100x microscope objective. Polarisation of the incident laser was set by half lambda plate to be parallel to the longitudinal direction of carbon fibres. Baseline correction was applied to obtain a flat baseline between 800 cm⁻¹ to 2000 cm⁻¹. The peak at 1350 cm⁻¹ (D-band) was fitted with a Lorentzian function, while the peak at 1590 cm⁻¹ (G-Band) was fitted with a Breit-Wigner-Fano (BWF) function. The I_D/I_G ratio was calculated from the height of the two peaks.

SEM. Images were taken with a Zeiss Sigma VP. The fibres were adhered to a carbon tape as conductive support and then sputter-coated with gold to ensure electric conductivity. To image the cross section the fibre bundle was fractured and then glued onto the conductive support. The images were taken at 3.00 kV operating voltage.

3. Results and discussion

3.1. SWV and CV results

A reversible electron transfer is well known for [Fe^{II/III}(CN)₆] at a freshly polished GCE and was recently reported for [Fe^{II/III}-racEDDHA].³⁵ Fig. 4 shows representative CVs of both redox carriers studied [Fe^{III}-racEDDHA] (a) and [Fe^{II}(CN)₆] (b) at a freshly polished GCE. The small peak separation of 68 mV for both couples demonstrates a reversible electron transfer.

In contrast to GC, CFs represent an anisotropic material and the microstructure depends strongly on the production conditions and on the fibre precursor (polyacrylonitrile, rayon, pitch).³⁸ The a-axis of the graphitic lattice is preferentially oriented along the fibre axis,³⁹ thus the lateral surface and the cross-section of a fibre may show different electrochemical response.⁴⁰ Post-spinning treatment, like anodic polarisation and application of sizing, alter the surface properties of CFs additionally. The structural differences thus require determination of the electron transfer properties for each chosen combination of redox couple and CF.

Determination of electrode transfer rates on carbon rovings using cyclic voltammetry is problematic.⁴¹ The Randles-Sevcik relation has been derived for planar electrodes in a semi-infinite diffusion field⁴² while CFs represent cylindrical microelectrodes. The arrangement of CF in a roving resembles an array of 3D microelectrodes forming a porous electrode structure. The peak separation in CV of porous electrodes is reduced, which makes interpretation of reversibility difficult.⁴³ The diffusion domain between the fibres is finite rather than semi-infinite and strongly depends on the macroscopic shape of the roving (embroidery etc).

CFMCEs made from single filaments were studied as a simplified model for carbon rovings. Due to cylindrical diffusion at CFMCE, CV cannot be used to determine the redox characteristics by simple methods.⁴⁴ For a Nernstian system SWV has shown to produce bell-shaped current potential curves where the peak shape does not depend on the size or geometry of the electrode.⁴⁵ SWV recorded with a cylindrical microelectrode feature a SWV of same shape and position compared to a planar electrode but with a higher peak current, which is a result of cylindrical diffusion.⁴⁶ In our work we utilised this geometric independence for qualitative comparison of CFMCE and GCE. As proposed by Singleton and co-workers⁴⁶ the peak half width (phw) of the net current in a SWV for a reversible electron transfer can be calculated from Eq. 4.

$$W_{1/2} = \left(\frac{RT}{nF}\right) \left[3.53 + 3.46 \left(\frac{nFE_{sw}}{RT}\right)^2 \left(\frac{nFE_{sw}}{RT} + 8.1\right) \right] = 123.8 \text{ mV} \quad (T = 296.2 \text{ K}; E_{sw} = 50 \text{ mV}) \quad (4)$$

Untreated and desized filaments exhibited poor electrochemical response with high variability in SWV (ESI-6). Chromic acid is reported to remove the sizing layer while leaving the bulk of the fibre and their mechanical strength unchanged⁴⁷ and was thus used as pretreatment for desized CFMCE. For the Fe^{II}/Fe^{III} redox couple a 100-fold increase of the rate constant has been reported after dipping in chromic acid.⁴⁸

The net currents of SWV experiments at GCE and CFMCE are depicted in Fig. 5. For better comparison the GCE data were normalised to the respective CFMCE current peak. The net currents of both electrodes superimpose, minimal deviations are attributed to the increasing baseline of the GCE. Excellent agreement between peak potential E_p (SWV) and half wave potential $E_{1/2}$ (CV) is observed as predicted from theory for a reversible electron transfer. The

increased peak half width and E_p of the CFMCE observed for [Fe^{II}(CN)₆] may be attributed to slight adsorption of impurities to which ultramicroelectrodes are prone. Voltammetric data for both redox couples and electrode types are depicted in Table 2.

Table 2. Cyclic voltammetry (CV) and square wave voltammetry of Na[Fe^{III}-racEDDHA] and K₄[Fe^{II}(CN)₆] at GCE and CFMCE (data extracted from Figure 4 and 5).

Technique	Electrode	Complex			
		[Fe ^{III} -racEDDHA]		[Fe ^{II} (CN) ₆]	
		ΔE_p mV	$E_{1/2}$ mV	ΔE_p mV	$E_{1/2}$ mV
CV	GCE	68	-623	68	223
		<i>phw</i> mV	E_p mV	<i>phw</i> mV	E_p mV
SWV	GCE	126	-617	124	223
	CFMCE	127	-621	129	235

The results demonstrate that both redox couples exhibit reversible electron transfer characteristics at the chosen CF after appropriate pretreatment.

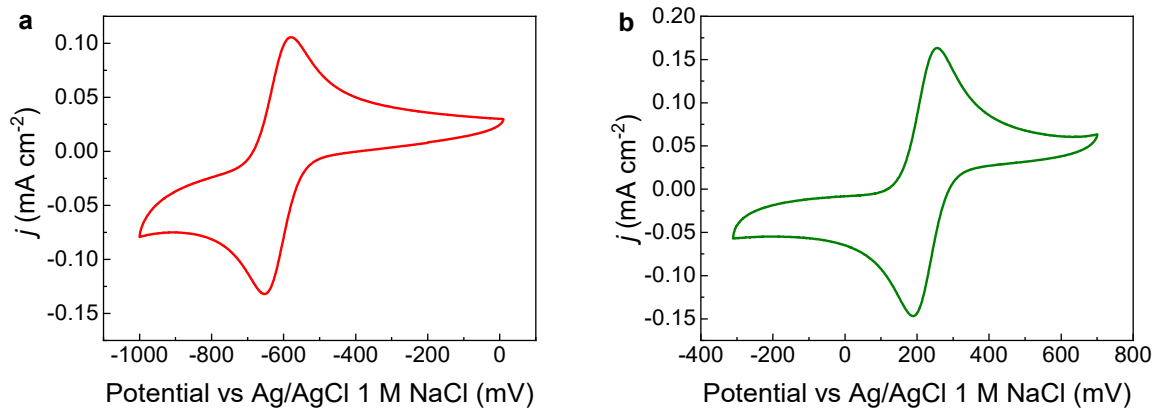


Fig. 4. CV at a polished GCE, scan rate 100 mVs⁻¹, (a) 1 mM Na[Fe^{III}-racEDDHA], (b) 1 mM K₄[Fe^{II}(CN)₆]; background electrolyte: 1 M Na₂SO₄, 5 mM borate, pH 9.

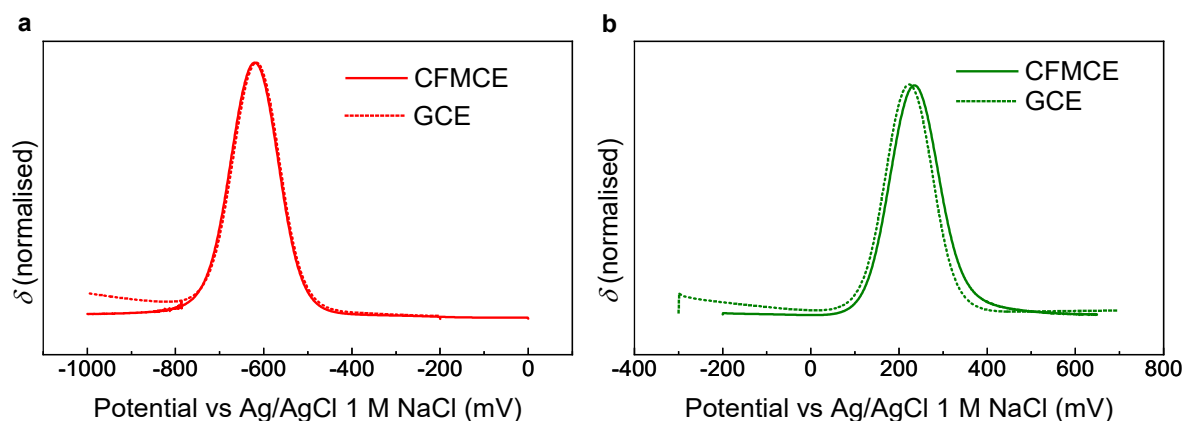


Fig. 5. Net currents (δ) of square wave voltammograms recorded at a polished GCE and chromic acid activated CFMCE ($E_{sw} = 50$ mV, $\Delta E_s = 1$ mV, 10 Hz), (a) 1 mM Na[Fe^{III}-racEDDHA], (b) 1 mM K₄[Fe^{II}(CN)₆]; background electrolyte: 1 M Na₂SO₄, 5 mM borate, pH 9.

3.2 Impedance Spectroscopy

EIS was used to evaluate the pretreatment of carbon rovings with regard to the electron transfer rate for both redox systems at 50% SoC. CRLEs served as simple disposable model for an embroidered 3D electrode. Since chromic acid activation showed good results at CFMCE, we additionally tested anodic activation as an alternative method. Optimisation of the anodic treatment with regard to polarisation time and potential is presented in ESI-7.

Due to the small activation polarisation resistance R_{ct} compared to the uncompensated resistance R_{hf} of typically 2 - 3 Ohms, a relatively large amplitude of 100 mV was applied to obtain well defined signals (ESI-8). For simulation of more realistic applicatory conditions the redox active species was set to 65 mM. The sodium sulphate concentration was limited to 0.7 M since higher concentrations lead to reduced solubility of Na[Fe^{III}-racEDDHA]. The reduction of the negative electrolyte will increase the pH,³⁵ thus a 2.4-fold excess of borate was chosen in order to maintain a stable pH. For the negative electrolyte 1 mM borate was sufficient to keep pH 9.

Fig. 6 shows representative Nyquist plots for both electrolytes using CRLEs after desizing and activation treatments (chromic acid or anodic polarisation). In order to obtain quantitative results for R_{ct} the impedance data were fitted to a Randles circuit (fitting data ESI-8) including a constant phase element (Q_{dl}) instead of a capacitor (see inset Fig. 6). The Warburg diffusion element (W) corresponds to the simplest diffusion situation, where the diffusion is unrestricted such as the case of a planar electrode. Deviations from the angle 45° are associated to non semi-infinite linear diffusion due to the electrode porosity.^{49,50}

Fig. 7 shows the effect of the activation process on the R_{ct} for both redox couples considered in this work. Due to the polymer coating of the pristine CF a considerably large value of R_{ct} is observed for the untreated CLRE. A reduction of R_{ct} to less than 4% of the initial value is already achieved through desizing by acetone extraction. The relatively large variations in R_{ct} of desized CLREs can be explained by presence of small residues of sizes on the roving surface. Oxidative activation leads to further decrease of R_{ct} to values $\leq 0.1 \Omega$

(0.023 Ω g), which is more pronounced for the ferrocyanide redox system. Similar reduction of R_{ct} was obtained with both anodic oxidation and with chromic acid oxidation. Considering the comparable performance of both activation methods, environmental and safety aspects, the electrochemical activation was selected for further experiments.

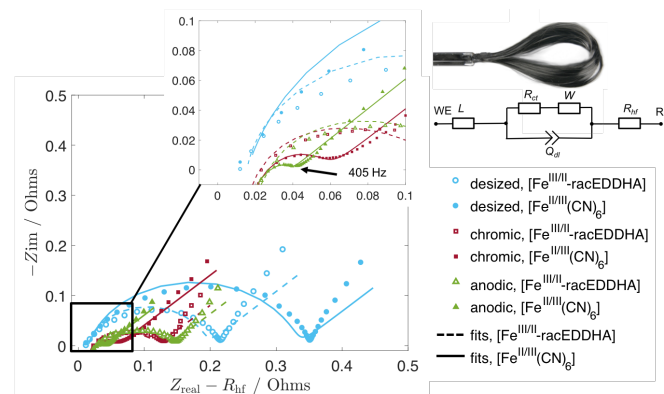


Fig. 6. Nyquist plot illustrating the effect of different activation processes on CRLEs. Desized (circles), chromic acid treated (squares), and anodically polarised at 1800 mV, 90 s, 0.1 M NaOH (triangles) CLRE. Solid symbols indicate electrolyte: 32.5 mM K₃[Fe^{III}(CN)₆], 32.5 mM K₄[Fe^{II}(CN)₆], 0.7 M Na₂SO₄, 1 mM Borate. Empty symbols indicate electrolyte: 50% SoC Na[Fe^{III}-racEDDHA].

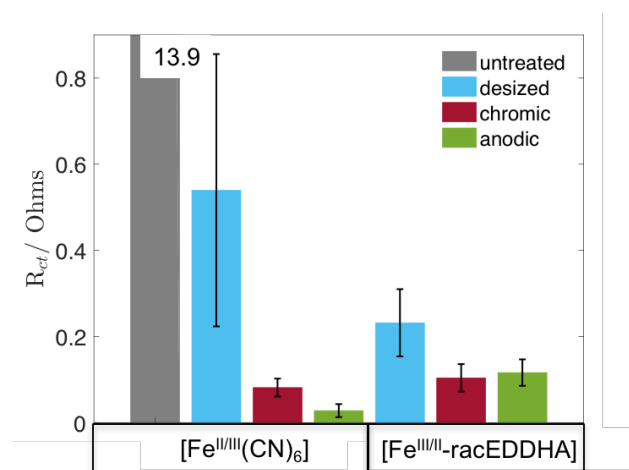


Fig. 7. Dependence of R_{ct} on activation treatment of CLREs, 65 mM metal complex 50% SoC, 0.7 M Na₂SO₄, 1 mM Borate, pH 9.

3.3. Cycling stability

Bulk electrolysis was conducted to test the performance of CRLEs under conditions of electrochemical turnover. A series of charge/discharge experiments was performed for the negative and the positive electrolyte separately. The coulombic efficiency (CE) was calculated from photometric and coulometric data according to Eq. 5, where n_{pt} are the number of moles obtained with photometry

(c is the concentration, V is the volume, and 0.8 is the SoC difference), and n_{ec} the number of moles calculated from Faraday's law (I is the current, t is the time and F is the Faraday's constant).

$$CE = \frac{dn_{pt}}{dn_{ec}} = \frac{0.8 \cdot c \cdot V}{I \cdot t \cdot F^{-1}} \quad (5)$$

The potential of the respective working electrode E_{we} and the electrolyte redox potential E_{sol} as function of charge/discharge cycles are shown in Fig. 8a,c. Averaged overpotentials ($\bar{\eta}$, see Eq. 3) and CE per cycle for [Fe^{III}-racEDDHA] and [Fe^{III}(CN)₆] are shown in Fig. 8b,d. In case of [Fe^{III}(CN)₆] a time stable value for $\bar{\eta}$ was obtained. In case of the [Fe-racEDDHA] complex even a slight decrease in $\bar{\eta}$ was observed. Thus, no deactivation of the carbon electrode surface was measured during repetitive cycling. Excellent CE was observed for both redox systems, indicating the absence of parasitic side reactions and suggesting a good electrochemical stability of all electrochemically active species. The applied procedure of desizing and anodic activation of the CRLE lead to formation of a stable and active carbon surface, which is not degraded or passivated during extended electrolysis. Independent on electrode potential, passivation was not observed in the potential window between +800 mV and -1200 mV vs Ag/AgCl, which demonstrates the high chemical stability of the surface towards electrochemical degradation processes at the chosen experimental conditions.

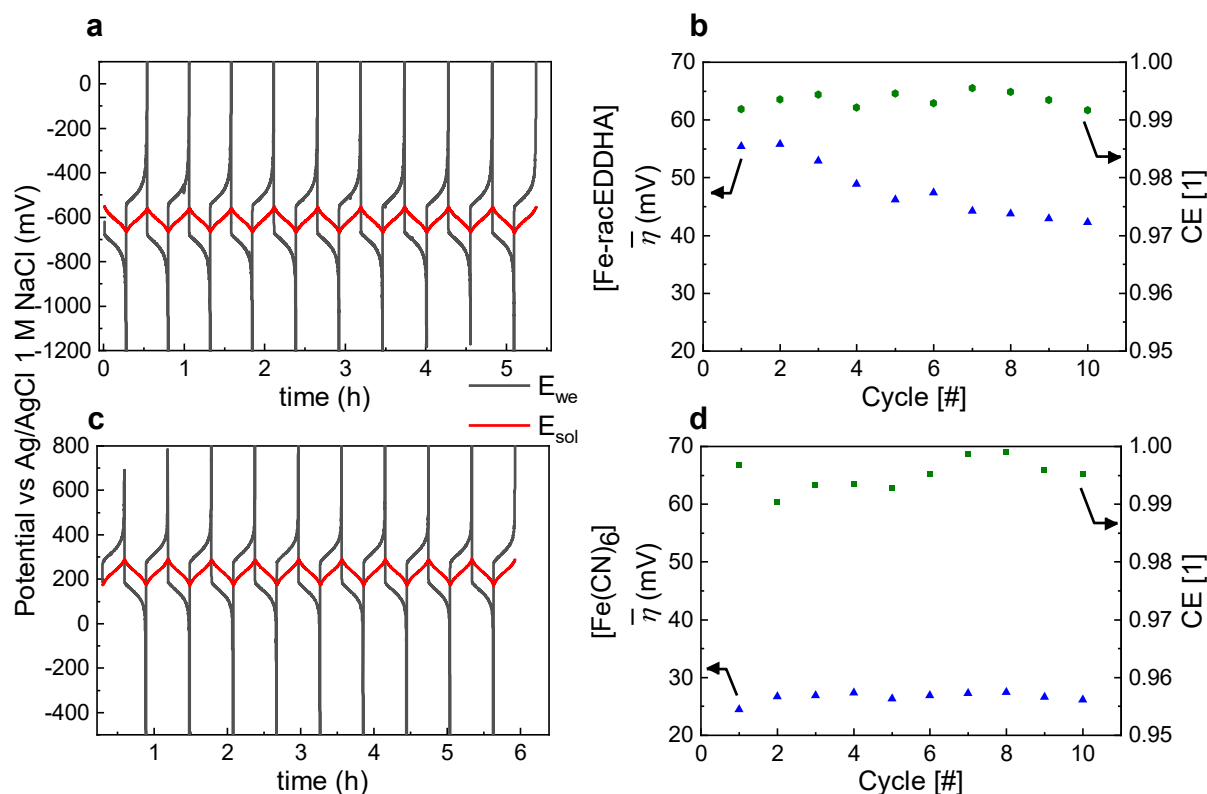


Fig. 8. Galvanostatic charge/discharge cycling experiment of [Fe^{III}-racEDDHA] (a,b) and [Fe^{III}(CN)₆] (c,d); E_{we} and E_{sol} vs time (a,c); $\bar{\eta}$ (calculated at 50% SoC) and CE vs cycle number (b,d); CLREs anodically activated (1800 mV, 90 s); 10 mM of Fe-complex; 10-90% SoC; cell current +/-50 mA.

3.4. Surface characterisation

SEM. The untreated fibre shows characteristic grooves running parallel to the fibre axis (Fig. 9). Patches of sizing compound are visible, and a homogeneous layer can be anticipated. After desizing, randomly distributed islands of sizing compound can be found, indicating an incomplete desizing process. Both oxidatively treated samples feature a clean and undamaged surface. These results confirm that the activation treatments removed residual sizing and did not damage the bulk or the surface of the fibre. Therefore, no significant weight loss was measured in the samples after the treatments.

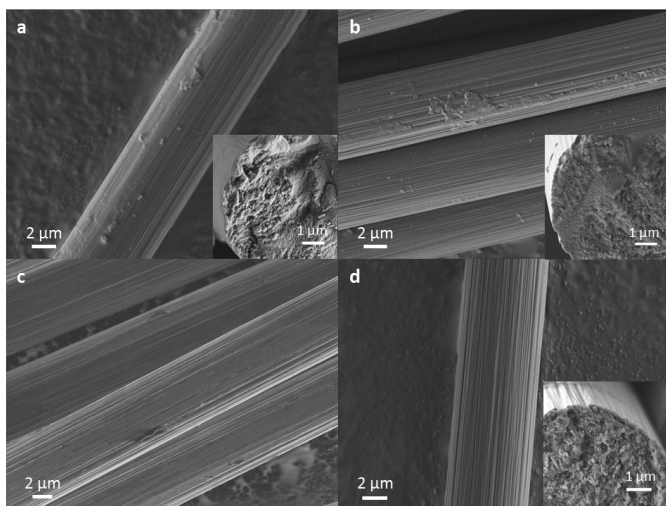


Fig. 9. SEM images of differently treated carbon fibres. Untreated (a), desized (b), chromic acid treated (c) and anodically activated (d) fibre. The insets show the cross section of the respective fibre (they can also be found in larger scale in ESI-9).

Raman spectroscopy. In Fig. 10a the Raman spectra in the wavenumber interval between 1200 cm^{-1} and 1800 cm^{-1} are shown. The ratio between the intensities of the D-band and G-band (I_D/I_G) is shown in Fig. 10b as a function of the respective activation treatment. Compared to graphite, which exhibits a value of I_D/I_G of 0.4 a higher value of I_D/I_G of 0.78 is observed, which indicates higher level of disorder and surface oxidation of the CFs. The influence of the different treatments on the I_D/I_G ratio however is not significant.^{51,52} Raman spectra of the CFs indicated only minor changes in the characteristic intensities⁵³ of the D-band I_D (located near 1350 cm^{-1}) and the G-band I_G (located near 1590 cm^{-1}). Thus, the surface of the pristine CFs was not altered by the oxidative treatments to an extent, which would lead to a distinct change in the ratio I_D/I_G .

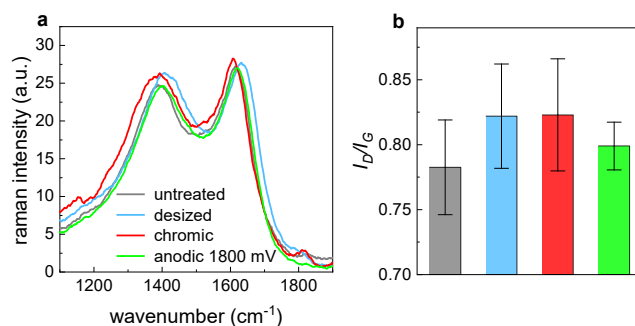


Fig. 10. Raman spectra (a) and ratio I_D/I_G (b) of untreated, desized and activated CRLE. Average of 5 measurements.

XPS. From XPS analysis, the elemental composition of the activated and the pristine CFs was determined (Table 3). In the pristine and desized CF samples a nitrogen content of about 2 atom% was found. The presence of surface nitrogen on the acetone extracted sample may be related to traces of residual sizing layer. The oxygen/carbon ratio is slightly reduced after desizing, while oxidative treatments reduce the surface nitrogen below the detection limit (Fig. 11 and ESI-10) and significantly increase the O/C ratio compared to the desized sample. This indicates formation of oxygen functional groups at the surface, which is especially visible on the chromic acid treated fibre.

Table 3. Elemental composition of CF as determined by XPS (b.d. = below detection limit) and quantification of the deconvoluted C 1s spectra.

	atomic percentage			O/C ratio	Peak deconvolution				
	C	O	N		sp^2	sp^3	C-N/C-O-C	C-OH	C=O
untreated	74	24	2	0.32	53	0*	44	0*	3
desized	77	22	2	0.29	64	0*	33	0*	3
chromic	72	28	b.d.	0.39	65	23	0	7	5
anodic (1.8 V)	74	26	b.d.	0.35	70	18	0	6	6

*Due to the small binding energy difference between C-N/C-O-C, C-C and C-OH the small contributions of C-C and C-OH species to the C-N/C-O-C signal cannot be excluded.

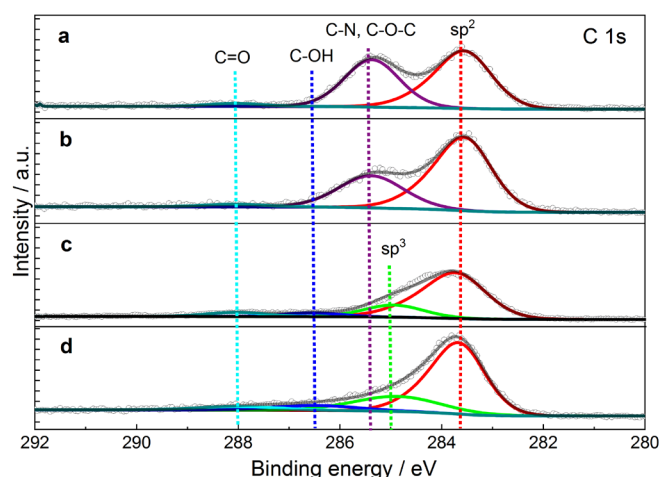


Fig. 11. Deconvolution of the C 1s spectra of the untreated sample (a), after desizing with acetone (b), after treatment with chromic acid (c) and after anodic polarisation treatment (d).

Deconvolution results of the C 1s spectra are shown in Fig. 11 and summarized in Table 3. A prominent sp^2 carbon peak can be observed for all fibre spectra at 283.6 eV (deconvolution data are listed in Table S8). By desizing the untreated sample with acetone, the overall O/C ratio decreases, and thus the C-N, C-O-C (285.4 eV)/ sp^2 carbon ratio appears smaller.⁵⁴

After further treatment (Fig. 11c,d), the C-N component cannot be observed anymore. However, a feature at 285.0 eV appears which is typical for C-C and C-H species. This suggests that the surface nitrogen is totally removed, and agrees well with the N 1s spectra shown in ESI-10, where no surface nitrogen is visible after the oxidative treatments. Additionally, more oxygen functionalities in the form of carbonyls are observed, which can be rationalized by the oxidative behaviour of chromic acid and the anodisation process. The O 1s spectra (ESI-10) confirms the clear increase of oxygenated species after oxidative treatments through the presence of additional O 1s components at the low binding energy side.

3.5. Effect of pretreatment on the electrode characteristics and performance

According to EIS, TGA, XPS and SEM experiments, a major part of the sizing layer is removed in the acetone extraction step. XPS and SEM experiments indicate residues of sizing, which is confirmed by relatively large R_{ct} of the desized samples in EIS experiments. Both oxidative treatments fully remove the residual sizing, but the decrease of R_{ct} is more pronounced for $[Fe(CN)_6]$ compared to $[Fe\text{-}racEDDHA]$. According to XPS measurements, chromic acid treated fibres feature a slightly higher concentration of carbonyl groups than anodically treated fibres. Hence, the larger R_{ct} values for $[Fe(CN)_6]$ may be derived from the additional negative excess charge on the surface, which may induce electrostatic repulsions that hinder the electron transfer.³⁹

Both, EIS and cycling experiments showed larger R_{ct} and $\bar{\eta}$ for $[Fe\text{-}racEDDHA]$ indicating slightly slower electron transfer, which is in contrast to the results of CV and SWV experiments. Since the coordination sphere changes in the redox process,³⁵ an increased reorganisation energy compared to $[Fe(CN)_6]$ could explain this

effect as reported recently for FeHEDTA.⁵⁵ Additionally, $\pi\text{-}\pi$ interactions between the aromatic groups of the ligand and the graphitic carbon surface could reduce the speed of electron transfer.

Besides its beneficial safety aspects, the anodic treatment offered comparable performance for the $[Fe^{II/III}\text{-}EDDHA]$ redox couple and slightly better performance for $[Fe^{II/III}(CN)_6]$ than the chromic acid treatment.

Conclusions

Embroidery techniques permit production of near net shaped carbon-based 3D electrodes using commercial carbon fibre rovings. For use in redox flow cells however the surface of the manufactured electrodes has to be activated to remove any polymer sizing layer and to achieve low overpotentials for a chosen electrolyte. Low charge transfer resistance of the carbon electrodes could be obtained by acetone extraction followed by an anodic oxidation in an alkaline electrolyte. Characterisation of the fibres with SEM and Raman spectroscopy indicated that the surface activation did not lead to irreversible damage of the fibre. XPS measurements showed that the sizing is fully removed after oxidative activation, accompanied by an increase of surface oxygen functional groups. From impedance spectroscopy on carbon roving loop electrodes a charge transfer resistance of $< 0.1 \Omega$ was determined for the 65 mM $[Fe^{II/III}(CN)_6]$ electrolyte and $< 0.2 \Omega$ for the 65 mM $[Fe^{II/III}\text{-}racEDDHA]$ electrolyte each at 50% SoC. No increase in overpotentials was observed in bulk electrolysis experiments during repetitive cycling of the electrolytes between 10% and 90% SoC, thus no losses in activation were observed in the potential window of -1200 mV to 800 mV vs Ag/AgCl. Therefore, cycling experiments demonstrated the stability of the treated electrodes over 10 cycles during 5-6 hours and at relatively high lower and upper SoC values. Further long-term experiments will be assessed in future work.

The use of carbon rovings as basis material which can be processed by embroidery techniques to near net shaped 3D electrodes followed by subsequent desizing and activation opens a new and highly useful technique to manufacture electrodes for redox flow cells and other electrochemical applications. In this work, activation of polyacrylonitrile-based CFs was studied. Various microstructures that show increased edge plane exposure are known for different pitch-based CFs.⁵⁶ Selecting CFs based on a favourable microstructure is expected to permit further improvement of the electrochemical performance.

Conflicts of Interest

The authors declare that they have no conflict of interest.

Acknowledgements

Author N.A.A. thanks the Austrian Science Fund (FWF) for the Project EmbelRed T-1041 funded under the Hertha Firnberg Programme. This research was financially supported by the Austrian research promotion agency (FFG) K-Project TCCV (860474) Textile Competence Center Vorarlberg. A.A. is a recipient of a doctorate

(DOC) Fellowship of the Austrian Academy of Sciences at the Institute of Physical Chemistry.

References

- 1 T. X. Huong Le, M. Bechelany and M. Cretin, *Carbon*, 2017, **122**, 564–591.
- 2 L. F. Castañeda, F. C. Walsh, J. L. Nava and C. Ponce de León, *Electrochim. Acta*, 2017, **258**, 1115–1139.
- 3 Y. Gao, H. Wang, Q. Ma, A. Wu, W. Zhang, C. Zhang, Z. Chen, X. X. Zeng, X. Wu and Y. Wu, *Carbon*, 2019, **148**, 9–15.
- 4 J. Vázquez-Galván, C. Flox, J. R. Jervis, A. B. Jorge, P. R. Shearing and J. R. Morante, *Carbon*, 2019, **148**, 91–194.
- 5 C. Kim, P. Srimuk, J. Lee, S. Fleischmann, M. Aslan and V. Presser, *Carbon*, 2017, **122**, 329–335.
- 6 D. J. Ahirrao and N. Jha, *Carbon*, 2019, **152**, 837–850.
- 7 R. L. McCreery, *Chem. Rev.*, 2008, **108**, 2646–2687.
- 8 P. Chen and R. L. McCreery, *Anal. Chem.*, 1996, **68**, 3958–3965.
- 9 C. E. Banks and R. G. Compton, *Anal. Sci.*, 2005, **21**, 1263–1268.
- 10 P. L. Runnels, J. D. Joseph, M. J. Logman and R. M. Wightman, *Anal. Chem.*, 1999, **71**, 2782–2789.
- 11 S. Ranganathan, T. C. Kuo and R. L. McCreery, *Anal. Chem.*, 1999, **71**, 2782–2789.
- 12 A. Z. Weber, M. M. Mench, J. P. Meyers, P. N. Ross, J. T. Gostick and Q. Liu, *J. Appl. Electrochem.*, 2011, **41**, 1137–1164.
- 13 C. Ding, H. Zhang, X. Li, T. Liu and F. Xing, *J. Phys. Chem. Lett.*, 2013, **4**, 1281–1294.
- 14 D. S. Aaron, Q. Liu, Z. Tang, G. M. Grim, A. B. Papandrew, A. Turhan, T. A. Zawodzinski and M. M. Mench, *J. Power Sources*, 2012, **206**, 450–453.
- 15 C. R. Dennison, E. Agar, B. Akuzum and E. C. Kumbur, *J. Electrochem. Soc.*, 2015, **163**, A5163–A5169.
- 16 N. Aguiló-Aguayo, T. Drozdziak and T. Bechtold, *Electrochem. commun.*, 2020, **111**, 1–5.
- 17 N. Aguiló-Aguayo and T. Bechtold, *J. Power Sources*, 2014, **254**, 224–231.
- 18 N. Aguiló-Aguayo, P. Pena Espiñeira, A. P. P. Manian, T. Bechtold, P. P. Espiñeira, A. P. P. Manian and T. Bechtold, *RSC Adv.*, 2016, **6**, 69685–69690.
- 19 P. Morgan, *Carbon Fibers and Their Composites*, CRC Press, Boca Raton, 1st ed., 2005.
- 20 L. H. Peebles, *Carbon fibers: formation, structure, and properties*, CRC Press, Boca Raton, 1st ed., 1995.
- 21 S. J. Park, *Carbon fibers*, Springer, Singapore, 2nd ed., 2018.
- 22 M. H. Kjell, E. Jacques, D. Zenkert, M. Behm and G. Lindbergh, *J. Electrochem. Soc.*, 2011, **158**, A1455–A1460.
- 23 A. M. Pezeshki, J. T. Clement, G. M. Veith, T. A. Zawodzinski and M. M. Mench, *J. Power Sources*, 2015, **294**, 333–338.
- 24 J. Maruyama, S. Maruyama, T. Fukuhara and K. Hanafusa, *J. Phys. Chem. C*, 2017, **121**, 24425–24433.
- 25 L. Yue, W. Li, F. Sun, L. Zhao and L. Xing, *Carbon*, 2010, **48**, 3079–3090.
- 26 B. Sun and M. Skyllas-Kazacos, *Electrochim. Acta*, 1992, **37**, 2459–2465.
- 27 W. Li, J. Liu and C. Yan, *Carbon*, 2011, **49**, 3463–3470.
- 28 J. Friedl, C. M. Bauer, A. Rinaldi and U. Stimming, *Carbon*, 2013, **63**, 228–239.
- 29 R. C. Engstrom, *Anal. Chem.*, 1982, **54**, 2310–2314.
- 30 A. Dekanski, J. Stevanović, R. Stevanović, B. Ž. Nikolić and V. M. Jovanović, *Carbon*, 2001, **39**, 1195–1205.
- 31 M. Pumera, T. Sasaki and H. Iwai, *Chem. - An Asian J.*, 2008, **3**, 2046–2055.
- 32 L. J. Kopley and A. J. Bard, *Anal. Chem.*, 1988, **60**, 1459–1467.
- 33 Y. Yi, G. Weinberg, M. Prenzel, M. Greiner, S. Heumann, S. Becker and R. Schlögl, *Catal. Today*, 2017, **295**, 32–40.
- 34 *AT Pat.*, EP19169602.0, 2019.
- 35 P. Schröder, D. Obendorf and T. Bechtold, *ChemElectroChem*, 2019, **6**, 3311–3318.
- 36 N. Fairley, *CasaXPS: Processing Software for XPS, AES, SIMS and More*, Casa Softward Ltd., 2009.
- 37 W. H. Gries, *Surf. Interface Anal.*, 1996, **24**, 38–50.
- 38 E. Frank, L. M. Steudle, D. Ingildeev, J. M. Spörl and M. R. Buchmeiser, *Angew. Chemie Int. Ed.*, 2014, **53**, 5262–5298.
- 39 R. L. McCreery, in *Electroanalytical Chemistry: A Series of Advances, Vol. 17*, ed. A. J. Bard, Marcel Dekker Inc., New York, 1991, pp. 221–374.
- 40 J. X. Feng, K. Renner, R. Kasser, R. N. Adams and M. Brazell, *Anal. Chem.*, 1987, **59**, 1863–1867.
- 41 T. Tichter, D. Andrae, J. Mayer, J. Schneider, M. Gebhard and C. Roth, *Phys. Chem. Chem. Phys.*, 2019, **21**, 9061–9068.
- 42 A. J. Bard and L. R. Faulkner, *Electrochemical Methods: Fundamentals and Applications, 2nd Ed.*, 2001.
- 43 D. Menshykau and R. G. Compton, *Electroanalysis*, 2008, **20**, 2387–2394.
- 44 K. Aoki, K. Honda, K. Tokuda and H. Matsuda, *J. Electroanal. Chem.*, 1986, **207**, 25–39.
- 45 K. Aoki, K. Tokuda, H. Matsuda and J. Osteryoung, *J. Electroanal. Chem.*, 1986, **207**, 25–39.
- 46 S. T. Singleton, J. J. O’Dea and J. Osteryoung, *Anal. Chem.*, 1989, **61**, 1211–1215.
- 47 D. M. Brewis, J. Comyn, J. R. Fowler, D. Briggs and V. A. Gibson, *Fibre Sci. Technol.*, 1979, **12**, 41–52.
- 48 R. J. Taylor and A. A. Humffray, *J. Electroanal. Chem.*, 1973, **42**, 347–354.
- 49 J. Bisquert, G. Garcia-Belmonte, F. Fabregat-Santiago and A. Compte, *Electrochem. commun.*, 1999, **1**, 429–435.
- 50 J. Bisquert and A. Compte, *J. Electroanal. Chem.*, 2001, **499**, 112–120.
- 51 A. Ferrari and J. Robertson, *Phys. Rev. B - Condens. Matter Mater. Phys.*, 2000, **61**, 14095–14107.
- 52 R. Muzyka, S. Drewniak, T. Pustelny, M. Chrubasik and G. Gryglewicz, *Materials (Basel)*, 2018, **11**.
- 53 M. A. Pimenta, G. Dresselhaus, M. S. Dresselhaus, L. G. Cançado, A. Jorio and R. Saito, *Phys. Chem. Chem. Phys.*, 2007, **9**, 1276–1290.
- 54 Y. Y. Smolin, M. Soroush and K. K. S. Lau, *Beilstein J. Nanotechnol.*, 2017, **8**, 1266–1276.
- 55 K. Obata, L. Stegenburga, Y. Zhou and K. Takanebe, *ACS*

- 56 *Sustain. Chem. Eng.*, 2019, **7**, 7241–7251.
D. D. Edie, in *Carbon Fibers Filaments and Composites*, eds.
J. L. Figueiredo, C. Bernardo, R. T. K. Baker and K. J.
Hüttinger, Springer Netherlands, Dordrecht, 1990, pp. 43–
72.